Separation and Purification Technology 283 (2022) 120233

Contents lists available at ScienceDirect

Separation and Purification Technology

journal homepage: www.elsevier.com/locate/seppur

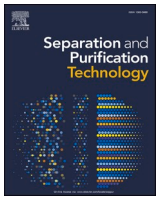

Masking covalent organic frameworks (COFs) with loose polyamide networks for precise nanofiltration

Zhe Zhang, Congcong Yin, Xiansong Shi, Guanghui Yang, Yong Wang *

State Key Laboratory of Materials-Oriented Chemical Engineering, College of Chemical Engineering, Nanjing Tech University, Nanjing 211816, PR China

ARTICLE INFO

Keywords:
Nanofiltration
Covalent organic frameworks (COFs)
Heterostructured membrane
Precise separation

ABSTRACT

Covalent organic frameworks (COFs) with uniform, tunable nanoporosities are promising alternatives to prepare nanofiltration membranes with homogeneous nanochannels for high-resolution molecular sieving. Due to the poor membrane-forming ability as well as the relatively inadequate strategies for pore engineering, thus far, the preparation of continuous and defect-free COF membranes with tunable pore sizes is still challenging. Herein, we demonstrate an ingenious strategy to prepare the heterostructured membranes featuring the loose polyamide networks masked COF nanofilms for precise sieving of small molecules. The loosely structured polyamides are created by the interfacial polymerization to mask the chemically stitched (chemically interlinked) ultrathin COF nanosheets. The masked polyamide with flexible, loose networks not only enhance the membrane-forming ability of the natively rigid ultrathin COF nanofilms, but also provide a masking effect that can effectively tune the pore size of the heterostructured COF membranes. Benefitting from the synergistic enhancement of the membrane-forming ability and the pore size tunability, thus-prepared membranes exhibit excellent molecular sieving performances toward various small molecules. This work is expected to provide a guidance for the rational design and controllable preparation of COF membranes for precise nanofiltration.

1. Introduction

Nanofiltration membranes featuring homogeneous nanochannels that can precisely sieve small molecules are of grand significance to chemical industry, energy harvesting and environmental remediation, are imminently demanded [1–3]. Two-dimensional (2D) covalent organic frameworks (COFs), a category of framework polymers, which are reticulated from the topologically structured building blocks to offer architectures with strict periodicity and regularity [4–7]. The well-defined structures endow COFs with appealing superiorities, such as intrinsic nanopores, tunable pore sizes, permanent nanoporosities, entirely organic backbones, flexibility for functionalizations. Alongside these features, most 2D COFs possess through pores with monodisperse nanopores tunable in the range of 0.64–5.3 nm [6], covering the region of nanofiltration (0.5–2 nm) [8]. Therefore, COFs have been recently emerged as more accessible alternatives for nanofiltration membranes toward the precise sieving of small molecules [9,10]. The pure COF membranes, of which the whole selective layers are made of COFs, are generally built from the bottom-up method including interfacial synthesis (polymerization) [11–14], in situ growth [15,16], stepwise growth [17,18], have demonstrated good separation properties to small molecules. However, thus far, the preparation of continuous and defect-free COF films with tunable pore sizes yet remains challenging.

To create crystalline COF films, the monomers are generally needed to be molecularly conjugated and have in-plane non-rotary groups, such as benzenes, triazines, and porphyrins [4]. Those characteristics would render COF structures permanent nanoporosities, however, leading to a highly rigid nature of the formed COF films. Besides, because the COFs are crystallized following the mechanism of nucleation and growth, while the nucleation kinetics is usually fast, relatively uncontrollable, and dominating the crystallization processes, inevitably spawning polycrystalline structures [19,20]. Those crystallites are anisotropically oriented, and randomly packed to produce the COF films, resulting in inhomogeneous microstructures [21]. Therefore, in most cases, the natively rigid structures along with the inhomogeneities will be problematic, as they would make the COF films brittle, fragile, and are prone to form defects, weakening the membrane-forming ability to create continuous selective layers on porous substrates.

In addition, the pore sizes of COF films are required to be tunable, which is essential for realizing the high precision separations. The pre-

* Corresponding author.
E-mail address: yongwang@njtech.edu.cn (Y. Wang).

https://doi.org/10.1016/j.seppur.2021.120233
Received 20 July 2021; Received in revised form 26 November 2021; Accepted 27 November 2021
Available online 1 December 2021

installation and post-modification of functional groups into the pore walls are the basic methods to continuously adjust the pore sizes of COF films [6]. However, these strategies usually rely on the *de novo* design and sophisticated synthesis of monomers, impeded them from large-scale fabrications. Very recently, the heterostructured COF films have risen as the viable alternative, the pore sizes of which can be continuously tuned in a controllable manner. During the pore engineering process, various nanomaterials are used to co-assemble with COFs, which is driven by the chemical or physical interactions, producing the heterostructured COF films with the mixed-dimensional configuration [22] or the bi-layered configuration [23–27]. The narrowed pore sizes would be created at the interface between those two co-assembled architectures. Thus, the incorporated nanomaterials can be regarded as the mask [28], in which the pore sizes can be exquisitely controlled via the regulation of the incorporation, stacking, off-set fashions of two co-assembled architectures so that to achieve the masking effect. Given the above, should the membrane-forming ability and the pore size tunability be synergistic enhanced, the COF membranes would be expected to fulfill the demand of the high-resolution separation toward small molecules.

Considering that the conventional polymers are in favourable membrane-forming ability, synergizing them with COFs would be a facile yet effective way to prepare continuous and defect-free COF membranes with tunable pore sizes. Herein, inspired by our previous works [29], we leveraged rigid COFs and flexible polyamides, the core materials for conventional nanofiltration membranes, to controllably prepare heterostructured COF membranes for precise sieving of small molecules (Scheme 1). Amino-COF nanosheets were chemically interlinked (chemical stitching) at the oil–water interface to form ultrathin nanofilms with their apertures perpendicularly oriented. Distinguished from the tightly structured polyamides as reported previously, the loosely structured polyamides were then created by the interfacial polymerization between piperazine and trimesoyl chloride in low concentrations to mask the underlying ultrathin nanofilms, yielding COF/PA heterostructured membranes. Benefitting from the masking of the loose and flexible polyamide chains, the rigid and ultrathin COF nanofilms with shape-persistent nanopores are capable of separating small molecules. The masking degree can be regulated by the forming durations of the polyamides, allowing the control of the pore sizes of the heterostructured membranes. Under the synergistic enhancement of membrane-forming ability and the pore size tunability, the heterostructured membranes demonstrated excellent sieving performances toward small molecules with different dimensions. This work delivers not only a strategy to endow rigid COFs with favourable membrane-forming ability by covering the loose polyamide networks, but also a masking effect to tune the pore sizes of the heterostructured membranes in the controllable manner, which is expected to achieve precise nanofiltration.

2. Experimental section

2.1. Materials

1,3,5-Triformylphloroglucinol (Tp, 95%) was provided by Tong-ChuangYuan Pharmaceutical. 3,3′-Dinitrobenzidine (BD-NO_2, 95%) was purchased from TCI. Tin (II) chloride dihydrate ($SnCl_2{\cdot}2H_2O$, 99%) was obtained from Macklin. Piperazine (PIP, 99%) was purchased from Alfa Aesar. Trimesoyl chloride (TMC, 98%), 4-(dimethylamino) pyridine (DMAP, 99%), and *n*-hexane (HPLC grade, >95%) were obtained from Sigma-Aldrich. Other chemical reagents including solvents, small organics, and inorganic salts were purchased from local suppliers. Unless otherwise specified, chemical reagents were analytical grade and used without further purification. Porous polyacrylonitrile (PAN) membranes, used as the substrates in this work, were prepared by the non-solvent induced phase separation (NIPS) process according to our previous work and exhibited the water permeance of ~ 1000 L m^{-2} h^{-1} bar^{-1} [29]. Deionized water (Conductivity < 5 μS cm^{-1}) was used throughout this work.

2.2. Preparation of TpBD-NH_2 nanosheets

According to our previous work [29], TpBD-NO_2 was synthesized by the polycondensation of Tp and BD-NO_2 under the solvothermal condition, and further converted into TpBD-NH_2 by the chemical reduction using $SnCl_2$. The TpBD-NH_2 nanosheets were prepared by the sonication-assisted liquid exfoliation of their bulks, and were presented in the form of an aqueous dispersion. The concentration of TpBD-NH_2 nanosheets was calculated by weighting TpBD-NH_2 nanosheets after being fully evaporated from their aqueous dispersion, which was ~ 0.01 mg mL^{-1}.

2.3. Membranes fabrication

The COF/PA membranes were fabricated via a two-step protocol based on our previous work (Fig. S1) [29]. To produce the TpBD-NH_2 nanofilms, the aqueous solution containing TpBD-NH_2 nanosheets (0.01 mg mL^{-1}) and DMAP (0.2 mg mL^{-1}), as well as the organic solution containing TMC (1 mg mL^{-1}) in *n*-hexane, were firstly prepared,

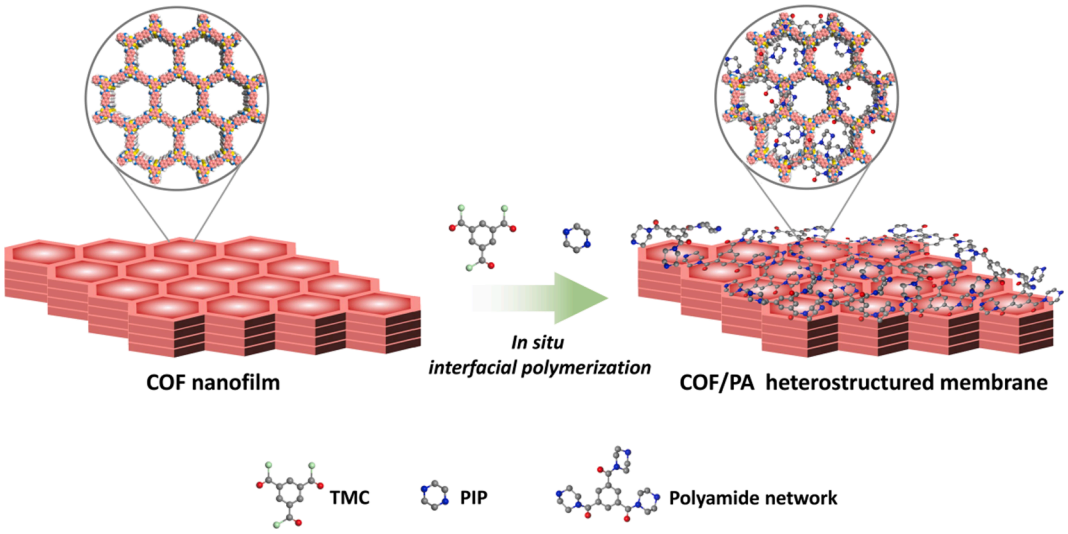

Scheme 1. Schematic illustration of the preparation of COF/PA heterostructured membranes.

respectively. Note that DMAP was used as a catalyst to initiate the acylation between amino groups of TpBD-NH_2 nanosheets and acyl chlorides of TMC, as the macrocyclic and conjugated structures of TpBD-NH_2 have a high steric hindrance. A square glass plate with an edge length of 6 cm was put on the bottom of a petri dish with 9 cm in diameter, after which 20 mL of the aqueous solution was added into the dish to fully immerse the glass plate. Then, 20 mL of the organic solution was gently poured out onto the upper surface of the aqueous solutions to trigger the reaction.

After the reaction proceeded for 30 s, 5 mL of the aqueous PIP solution was carefully injected into the above-mentioned aqueous solution along the wall surface of the dish using a syringe. The injection was maintained within a duration of 30 s. The final PIP concentration in the aqueous solution was 0.5 mg mL^{-1}. The subsequent reaction lasted for another 3, 5, 7, 10, and 15 min to create the COF/PA nanofilms at the interface between the aqueous and organic solution. The COF/PA nanofilms were gently picked up with the glass plate, and transferred onto the surface of a water bath, producing free-standing COF/PA nanofilms floating on water surface. Such nanofilms were further transferred to PAN substrates (COF/PA membranes), followed by a heat treatment at 60 °C for 10 min to reinforce the adhesion and mechanical stability.

The COF/PA membranes prepared with the forming durations of 3, 5, 7, 10, and 15 min were termed as COF/PA-3, COF/PA-5, COF/PA-7, COF/PA-10, and COF/PA-15, respectively. The control membrane without TpBD-NH_2 nanofilm (PA membrane) was prepared by the similar procedure, in which 0.5 mg mL^{-1} of the PIP aqueous solution reacted with 1 mg mL^{-1} of the TMC organic solution with a duration of 7 min.

2.4. Characterizations

X-ray diffraction (XRD) patterns of COFs were recorded at room temperature on a Smart Lab diffractometer (Rigaku). The patterns were collected in a 2θ range of 2 to 30°, with a scanning step of 0.02 s^{-1}. High-resolution transmission electron microscopy (HRTEM) observations of COFs were performed on a Tecnai G2 F30 S-Twin microscope (FEI) operating at 300 kV. Nanosheet dispersions were dropped over a TEM grid. The height profiles of the samples were determined on a XE-100 atomic force microscopy imaging system (AFM, Park Systems) operating at a scanning rate of 0.5 Hz. Samples were attached onto the silicon wafers. Scanning electron microscopy (SEM) observations of membranes were conducted on a S-4800 microscope (Hitachi) operating at an accelerating voltage of 3 kV. To reduce the discharging effect, the membranes were evenly sputtered of an ultrathin layer of gold prior to imaging. Water contact angles (WCAs) of membranes were recorded on a Drop Meter A100P goniometer (MAIST). At least five sites of each membrane were measured to obtain the average angle. Zeta potentials of membranes were performed on a SurPASS electrokinetic analyzer (Anton Paar GmbH) under the streaming potential method. 0.1 mM of KCl solutions were adopted as the background electrolyte solutions. The pH values during the test were adjusted by 0.1 M HCl and NaOH aqueous solutions, respectively. The chemical compositions of membranes were analyzed by attenuated total reflectance Fourier transform infrared spectroscopy (ATR-FTIR, Nicolet 8700, Thermo Fisher Scientific), and X-ray photoelectron spectroscopy (XPS, K-Alpha, Thermo Fisher Scientific), respectively.

2.5. Nanofiltration performance evaluation

The nanofiltration performances of membranes were tested in a dead-end filtration cell (Amicon 8003, Merck Millipore) under a hydraulic pressure of 2.5 bar. The membranes were compacted at 2.5 bar for 30 min to stabilize the water permeance prior to testing. The concentration of the small organic solutions was 50 ppm. For the mixture solutions, the concentration of the individual organic was 25 ppm. The concentration of the inorganic salts solutions was 1000 ppm. The permeation flux (J, L $m^{-2}h^{-1}$) and permeance (L $m^{-2}h^{-1}$ bar^{-1}) were calculated as following:

$$J = \Delta V/(A\ \Delta t) \tag{1}$$

$$Permeance = J/\Delta p \tag{2}$$

where ΔV (L) is the volume of the filtrate, A (m^2) is the effective filtration area, Δt (h) is the filtration duration, and Δp (bar) is the hydraulic pressure across the membrane.

The rejection rates of the small organics and the inorganic salts (R, %) were calculated as follows:

$$R = \left(1\ - C_p/C_f\right) \times 100\% \tag{3}$$

where C_p and C_f are the concentrations of the permeated and the feed solutions, respectively. The concentrations of the small organics and the inorganic salts were determined by a Nanodrop 2000c UV–vis spectrophotometer (Thermo Fisher Scientific) and a S230-K electrical conductivity meter (Mettler-Toledo), respectively.

3. Results and discussion

To create COF/PA heterostructured membranes, we prepared the TpBD-NH_2 nanosheets according to the previous work [29]. The amino groups of TpBD-NH_2 nanosheets provide reactive sites to interlink with TMC forming amide bonds. The diffraction peaks of (1 0 0) and (0 0 1) crystallographic planes in XRD patterns reveal the highly crystalline nature of the COFs (Fig. S2). Besides, the lattice fringes belonging to the (1 0 0) crystallographic plane also appear in the HRTEM image (Fig. S3). We then used the ~ 4 nm-thick TpBD-NH_2 nanosheets to prepare the nanofilms at the oil–water interfaces by the chemical stitching, and a ~ 4.5 nm-thick TpBD-NH_2 nanofilm was thus obtained (Fig. S4 and S5). However, because of the natively rigid nature, such ultrathin nanofilm was in insufficient mechanical strength. After being composited with substrates, the cracks and defects can be obviously seen throughout the nanofilm (Fig. S6), and it could not be directly used as the separation membrane.

To address this issue, we created flexible polyamide networks to mask the brittle TpBD-NH_2 nanofilm, forming the COF/PA heterostructured membranes. The polyamide networks are created by interfacial polymerization between TMC and PIP after the formation of the TpBD-NH_2 nanofilm. Owing to the reaction–diffusion process of interfacial polymerization, the pre-formed TpBD-NH_2 nanofilm are capable of mediating the diffusion of PIP toward the organic phase. Thus, the polyamide networks are mainly formed upon the upper surface of the nanofilm, or, put another way, the underlying TpBD-NH_2 nanofilms are partially encapsulated by the polyamide networks. In our previous work [29], the polyamide networks are in tight structure with the high rejection to ions. For the separation of small molecules, of which the molecular dimensions are larger than those ions, the polyamide networks are needed to be loosely structured. Otherwise, the tortuous sub-/nano pores inside polyamide networks would work as the primary sieving channels instead of the intrinsic pores of TpBD-NH_2. Considering that the TMC reacted with TpBD-NH_2 nanosheets and PIP molecules successively, the TMC with a low concentration was used to lower the reactivity between TMC and PIP, thus producing TpBD-NH_2 nanofilms masked with a layer of loose polyamide networks. The nanofilm can be floated on the water surface, and no cracks or tears can be seen by the naked eye, evidencing its excellent mechanical strength (Fig. 1a). The free-standing nanofilm can be further transferred, and composited onto the PAN substrate, without compromising its structural integrity (Fig. 1b). We then used SEM to analyze the morphologies of thus-prepared membranes. The COF/PA membranes do not have any defects, and the wrinkles along with the flat surface can be clearly observed (Fig. 1c and S7). In contrast, the control PA membrane

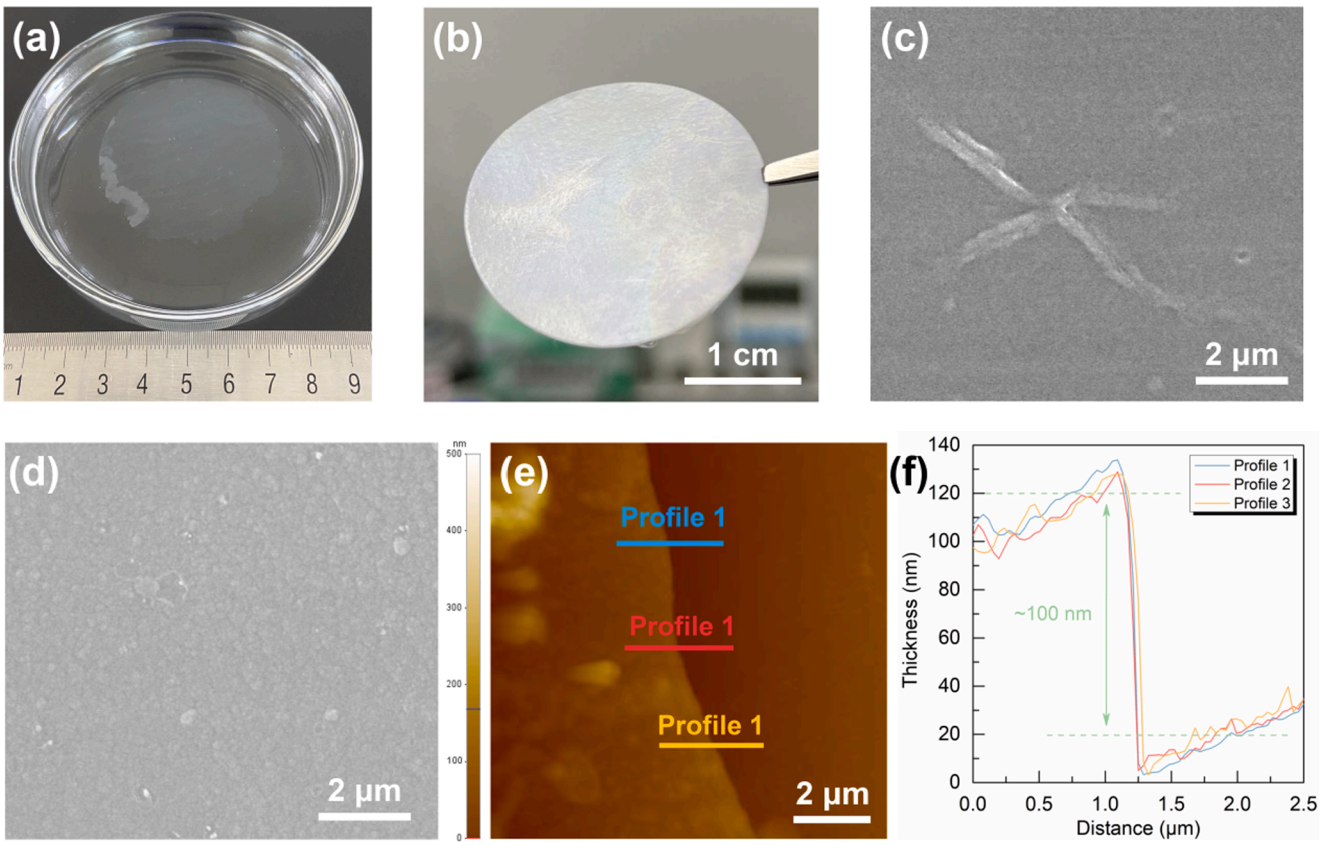

Fig. 1. Characterizations of membranes. (a) COF/PA-10 nanofilm floating on water. (b) COF/PA-10 nanofilm composited on the PAN substrate. (c) SEM image of the surface morphology of COF/PA-10 membrane. (d) SEM image of the surface morphology of PA membrane. (e) AFM image of COF/PA-10 nanofilm. (f) Height profiles of COF/PA-10 nanofilm.

exhibited a typical nodule-like morphology (Fig. 1d), which usually appears in conventional polyamide nanofiltration membranes. This discrepancy can be attributed to the mediation effect of TpBD-NH_2 nanofilm, the nanopores of which retarded the diffusion kinetics of PIP molecules toward the organic phase during interfacial polymerization, making the reaction more controllable [30–33]. Overall, the loose polyamide networks can significantly enhance the structural integrity of the ultrathin TpBD-NH_2 nanofilms.

To further analyze the microstructures of the membranes, we investigated the nanofilm thicknesses by AFM imaging (Fig. 1e and f, Fig. S8). All the COF/PA nanofilms possess analogous thicknesses of ~ 100 nm which could be explained as following: To form the loosely structured polyamide networks, the low concentration of TMC was used. Because the TMC would react with TpBD-NH_2 nanosheets and PIP molecules in sequence, thus a large part of TMC molecules were consumed in the formation of the TpBD-NH_2 nanofilms. Subsequently, TMC with significantly reduced concentration reacted with PIP molecules, resulting in a large number of non-bonded polyamide chains. Thus-formed networks are loosely structured, rather than tightly structured, which may pose spatially expanded architectures to present enlarged thicknesses. In addition, compared to the thick nanofilms of COF/PA, the control PA membrane exhibited a thickness of ~ 40 nm. It is indicated that without the mediation of TpBD-NH_2 nanofilms, the formation of polyamide networks was in a relatively uncontrollable manner, and the self-limiting effect would result in the very thin thickness. Overall, the low concentration of TMC generated the COF/PA nanofilms with similar morphologies and thicknesses.

To understand the structure–property relationship between the microstructures of membranes and the separation performances, we conducted the nanofiltration tests. A series of small organics were selected as the model solutes including dyes, active pharmaceutical ingredient (API), organic contaminant, and their dimensions and chemical structures are shown in Fig. 2a. We firstly studied the effects of different forming durations of polyamide networks on the separation performances (Fig. 2b). A neutrally charged API molecule with a dimension approaching to the intrinsic pore size of TpBD-NH_2 (1.7 nm), vitamin B-12 (VB-12, 1.8 nm × 1.7 nm), was adopted as the probe molecule to convincingly determine the size-based separation performances. As the forming duration was 3 min, the membrane showed a water permeance of ~ 30 L $m^{-2}h^{-1}$ bar^{-1} and a rejection rate of ~ 36%. The low rejection rate suggests that the continuous membranes were not formed, and the existing defects would compromise the rejection. When the forming duration increasing to 5 min, the membrane exhibited a water permeance of ~ 16 L $m^{-2}h^{-1}$ bar^{-1} and a rejection rate of ~ 90%. This result indicates that the relatively continuous membrane was formed, and the defects almost disappeared. With the forming duration to 7 min, the membrane showed a water permeance of ~ 13 L $m^{-2}h^{-1}$ bar^{-1} and a rejection rate of ~ 92%. Note that, when the forming duration increasing from 5 to 7 min, the membrane does not demonstrate very significant variations of water permeance and VB-12 rejection. Further increasing the forming duration to 10 min, the membrane exhibited a significantly declined water permeance of ~ 6 L $m^{-2}h^{-1}$ bar^{-1} and a rejection rate of up to ~ 98%. Finally, increasing the forming duration to 15 min, the water permeance of the membrane decreased to ~ 4 L $m^{-2}h^{-1}$ bar^{-1} and the rejection rate was in unchanged. Interestingly, with the forming duration increasing from 5 to 15 min, all the membranes consistently exhibited high rejection rates (higher than 92%), while the water permeances were gradually declined. Therefore, we understand the microstructure evolution of the COF/PA membranes. Because the retarded diffusion makes the PIP molecules very difficult to adequately react with TMC to form continuous membranes at the short forming duration, the COF/PA membranes were defective. When the

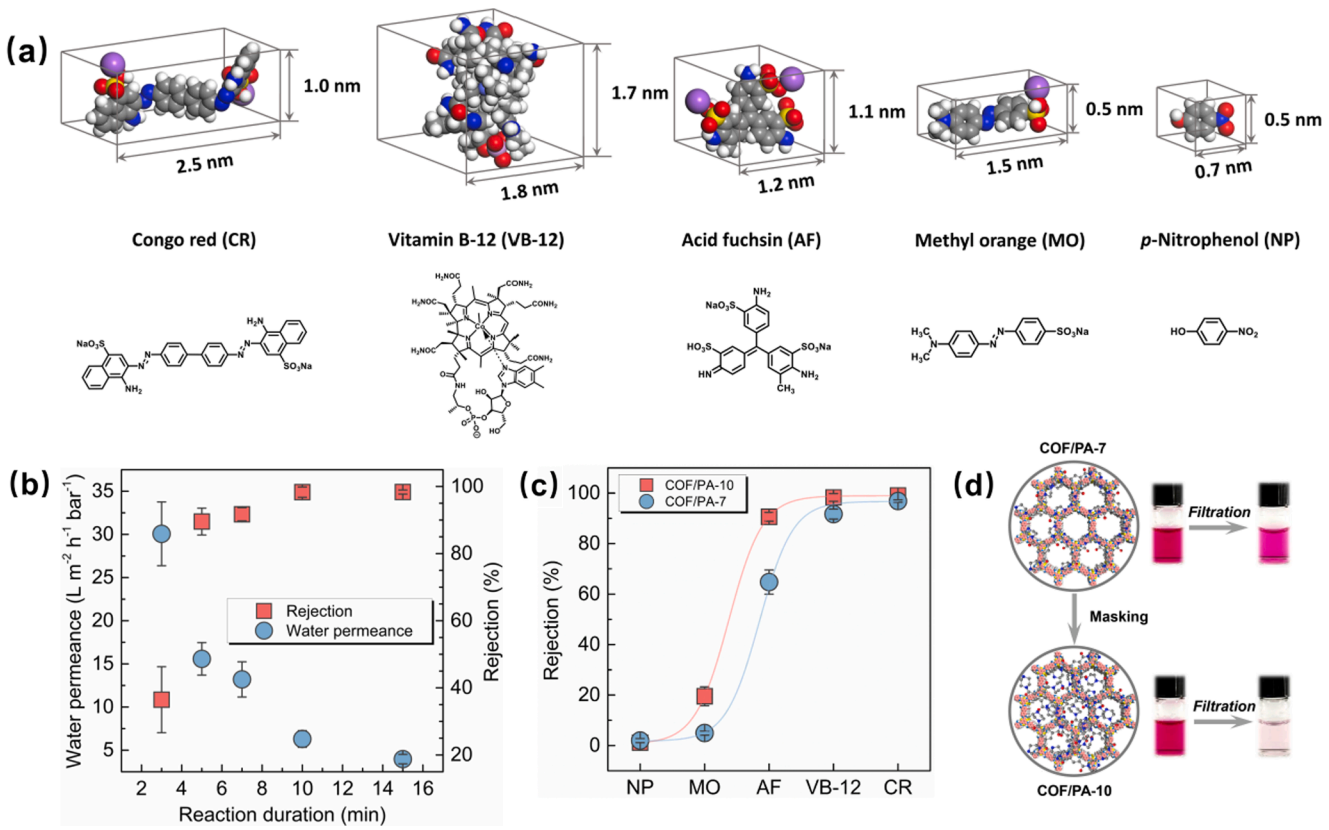

Fig. 2. Nanofiltration performances. (a) Dimensions and chemical structures of various small organics. (b) Variation of water permeance and VB-12 rejection under different forming durations. (c) Rejection characteristics of COF/PA membranes toward various small organics. (d) Schematic illustration of the masking effect.

forming duration increased from 5 to 15 min, the water permeances were declined and the rejection rates were improved. Considering that the membrane thicknesses were in unchanged during the formation of the polyamide networks, thereby, the microstructures of the membranes are likely to be evolved from the loose structure to the tight structure, which will be discussed in detail later.

The COF/PA membrane forming at 7 min showed a rejection rate of ~ 92% to VB-12, thus, under such circumstance, the nanopores of TpBD-NH_2 can be regarded as the primary sieving channels. However, with the forming duration to 10 min, the COF/PA membrane exhibited a rejection rate of ~ 98%, therefore, the sieving effect was co-dominated by the nanopores of TpBD-NH_2 as well as the loosely structured polyamide networks upon them. The loosely structured polyamide networks acted as the mask, in which the polymer chains can partially mask the nanopores of TpBD-NH_2 to narrow the sizes of the primary transport channels lower than 1.7 nm. The masking effect could be manipulated by the forming duration, allowing the control over separation performances. To further elucidate the masking effect, we investigated the rejection characteristics of COF/PA membranes forming at 7 and 10 min toward small organics with different dimensions (Fig. 2c and d). The two membranes exhibited high rejection rates to Congo red (CR) and VB-12, while very low rejection rates to methyl orange (MO) and *p*-nitrophenol (NP). This unique sharp selectivity can be ascribed to the highly regular nanopores of TpBD-NH_2 [34,35], distinguished them from the amorphous polymeric membranes. Moreover, the two membranes demonstrated a distinctive discrepancy for the rejection of the acid fuchsin (AF): the COF/PA-10 exhibited a rejection rate of ~ 90% while the COF/PA-7 is ~ 60%. This result can be attributed to the masking effect as we have mentioned above. In the case of COF/PA-7, the PA networks possess abundant loose chains which is beneficial to the exposure of intrinsic pores of TpBD-NH_2. Thus, AF with a small dimension (1.2 nm × 1.1 nm) could not be effectively rejected by COF/PA-7. However, as the loose structure becomes tighter, the transport channels of TpBD-NH_2 were largely masked to give a narrowed sieving channel. Thus, the high rejection to AF achieved. Besides, as demonstrated by the UV–vis spectra (Fig. S9), the concentrations of retentate were higher than those of the feed, indicating that the separation processes were mainly driven by the size exclusion rather than the adsorption.

To better understand how the loosely structured polyamide influence the nanopores of TpBD-NH2, we performed ATR-FTIR and XPS analysis. The chemical compositions of the COF/PA membrane were verified by the ATR-FTIR spectra (Fig. S10). In the XPS spectra, the elements of C, N, O can be detected in both COF/PA-7 and COF/PA-10 membranes, and the element ratios of O and N (term as O/N ratio) were calculated to be 2.0 and 1.9, respectively (Fig. 3a). The O/N ratio can be described based on the typical theory for the formation of polyamide network by interfacial polymerization [36]. The three acyl chloride groups of TMC completely react with the amines to form the segment with three O elements and three N elements, giving the fully cross-linked structure with the O/N ratio of 1 (Fig. 3b). The two acyl chloride groups of TMC react with the amines, while the residual was hydrolyzed into the carboxyl group, forming the segment with four O elements and two N elements, that is, producing the fully linear structure with the O/N ratio of 2 (Fig. 3c). Therefore, it can be concluded that COF/PA-7 and COF/PA-10 were loosely structured. Note that, the O/N ratio of COF/PA-10 is relatively lower than that of COF/PA-7, indicating the polyamide network of COF/PA-10 was tighter than that of COF/PA-7. This structure property (pore size tunability) is consistent with the AF rejection performances as mentioned above. It should also be noted that the pure polyamide networks are not likely to be in the fully linear structures. This is because the high values of O/N ratio could also be affected by a small quantity of TpBD-NH_2 nanosheets discretely embedded in the polyamide networks. Nevertheless, the loosely structured polyamide networks can be appropriately verified by the XPS analysis. Moreover,

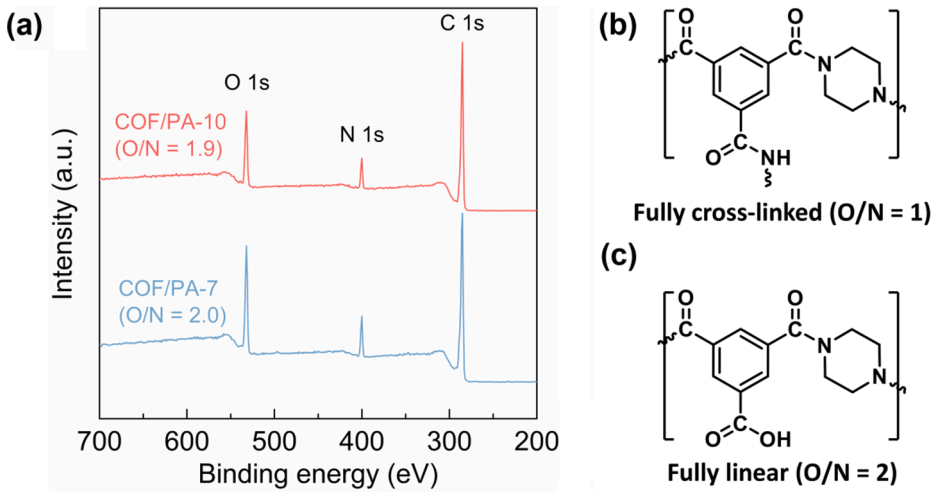

Fig. 3. XPS analysis. (a) The XPS spectra of COF/PA membranes. (b) and (c) Chemical structures of polyamide networks.

because the polyamide network of COF/PA-7 was looser than that of COF/PA-10, the COF/PA-7 bears much more carboxyl groups than that of COF/PA-10. This makes the COF/PA-7 more negatively charged (Fig. S11a). The loose structures also make the COF/PA-7 and COF/PA-10 membrane more hydrophilic than the control PA membrane (Fig. S11b).

After the elucidation of the structure–property relationship, to intuitively demonstrate the excellent molecular sieving characteristics, the COF/PA-10 membrane was challenged to sieve a mixture containing both neutral molecules of VB-12 and NP. After the nanofiltration, the two molecules can be completely separated, as verified by the color changes and the UV–vis spectra (Fig. 4a and b). Besides, to further demonstrate the successful creation of loosely structured polyamide networks, we used the COF/PA membranes and the control PA membrane to desalinate the inorganic salt solutions. As expected, the PA membrane demonstrated excellent desalination performances, while the COF/PA membranes were not able to desalinate the inorganic salt solutions (Fig. S12a). We then tested the separation performance of PA membrane to the small organics, as also expected, the control PA membrane can reject all those organics except NP (Fig. S12b). Above results, once again, prove the loosely structured polyamide networks are successfully created. Furthermore, the COF/PA-10 membrane exhibited an excellent long-term nanofiltration stability, as its permeation flux and rejection rate were in stable during a continuous filtration period for 30 h (Fig. 5).

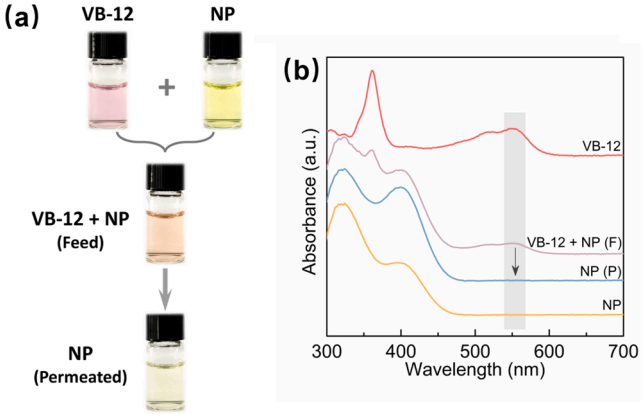

Fig. 4. Molecular-sieving characteristics of COF/PA-10. (a) Digital images of the small organic solutions before and after the nanofiltration. (b) UV–vis spectra of the small organic solutions before and after the nanofiltration.

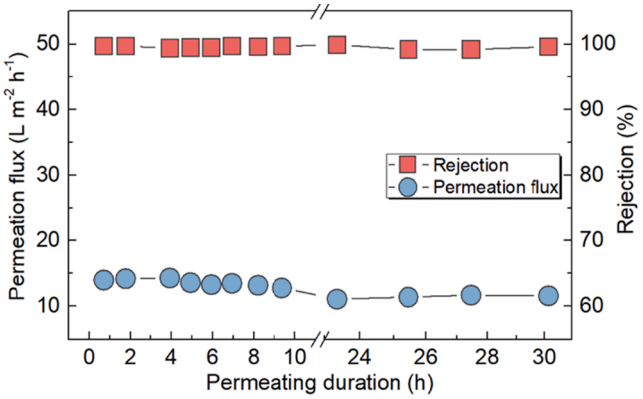

Fig. 5. Nanofiltration stability of COF/PA-10 membrane.

4. Conclusions

In summary, we reported a distinctive strategy to synergistically enhance the membrane-forming ability and the pore size tunability of the COF membranes via the creation of the loosely structured polyamide networks masked ultrathin COF nanofilms. TpBD-NH_2 nanosheets with the ~ 1.7 nm-sized nanopores were chemically stitched into ultrathin nanofilms, and further be masked with loose polyamide chains, yielding the COF/PA heterostructured membranes. Benefitting from the masking of the loose, flexible polyamide networks, the natively rigid ultrathin TpBD-NH_2 nanofilms with uniformly distributed nanopores are able to be used as molecular sieving membranes. By means of the regulation of forming duration of the polyamide, the pore sizes can be effectively tuned, which is capable of precisely sieving of small organic molecules in different dimensions. This work paves the way for the preparation of continuous and defect-free COF membranes with tunable pore sizes, which would be of great interest for the rational design and controllable construction of advanced COF membranes for diverse applications.

CRediT authorship contribution statement

Zhe Zhang: Conceptualization, Methodology, Investigation, Writing – original draft. **Congcong Yin:** Investigation. **Xiansong Shi:** Writing – review & editing. **Guanghui Yang:** Writing – review & editing. **Yong Wang:** Supervision, Writing – review & editing, Funding acquisition.

Declaration of Competing Interest

The authors declare that they have no known competing financial interests or personal relationships that could have appeared to influence the work reported in this paper.

Acknowledgements

This work was funded by the National Natural Science Foundation of China (21825803, 21921006).

Appendix A. Supplementary material

Supplementary data to this article can be found online at https://doi.org/10.1016/j.seppur.2021.120233.

References

[1] H. Dou, M.i. Xu, B. Wang, Z. Zhang, G. Wen, Y. Zheng, D. Luo, L. Zhao, A. Yu, L. Zhang, Z. Jiang, Z. Chen, Microporous framework membranes for precise molecule/ion separations, Chem. Soc. Rev. 50 (2) (2021) 986–1029.
[2] H.B. Park, J. Kamcev, L.M. Robeson, M. Elimelech, B.D. Freeman, Maximizing the right stuff: the trade-off between membrane permeability and selectivity, Science 356 (2017) 1138–1148.
[3] P. Liu, J. Hou, Y.i. Zhang, L. Li, X. Lu, Z. Tang, Two-dimensional material membranes for critical separations, Inorg. Chem. Front. 7 (13) (2020) 2560–2581.
[4] R. Liu, K.T. Tan, Y. Gong, Y. Chen, Z. Li, S. Xie, T. He, Z. Lu, H. Yang, D. Jiang, Covalent organic frameworks: an ideal platform for designing ordered materials and advanced applications, Chem. Soc. Rev. 50 (1) (2021) 120–242.
[5] D. Jiang, Covalent organic frameworks: an amazing chemistry platform for designing polymers, Chem 6 (10) (2020) 2461–2483.
[6] K. Geng, T. He, R. Liu, S. Dalapati, K.T. Tan, Z. Li, S. Tao, Y. Gong, Q. Jiang, D. Jiang, Covalent organic frameworks: design, synthesis, and functions, Chem. Rev. 120 (16) (2020) 8814–8933.
[7] A.P. Côté, A.I. Benin, N.W. Ockwig, M. O'Keeffe, A.J. Matzger, O.M. Yaghi, Porous, crystalline, covalent organic frameworks, Science 310 (5751) (2005) 1166–1170.
[8] J.R. Werber, C.O. Osuji, M. Elimelech, Materials for next-generation desalination and water purification membranes, Nat. Rev. Mater. 1 (2016) 1–15.
[9] C. Zhang, B.-H. Wu, M.-Q. Ma, Z. Wang, Z.-K. Xu, Ultrathin metal/covalent-organic framework membranes towards ultimate separation, Chem. Soc. Rev. 48 (14) (2019) 3811–3841.
[10] H. Wang, M. Wang, X.u. Liang, J. Yuan, H. Yang, S. Wang, Y. Ren, H. Wu, F. Pan, Z. Jiang, Organic molecular sieve membranes for chemical separations, Chem. Soc. Rev. 50 (9) (2021) 5468–5516.
[11] K. Dey, M. Pal, K.C. Rout, S. Kunjattu H, A. Das, R. Mukherjee, U.K. Kharul, R. Banerjee, Selective molecular separation by interfacially crystallized covalent organic framework thin films, J. Am. Chem. Soc. 139 (37) (2017) 13083–13091.
[12] W. Zhang, L. Zhang, H. Zhao, B. Li, H. Ma, A two-dimensional cationic covalent organic framework membrane for selective molecular sieving, J. Mater. Chem. A 6 (27) (2018) 13331–13339.
[13] R. Wang, X. Shi, A. Xiao, W. Zhou, Y. Wang, Interfacial polymerization of covalent organic frameworks (COFs) on polymeric substrates for molecular separations, J. Membr. Sci. 566 (2018) 197–204.
[14] R. Wang, X. Shi, Z. Zhang, A. Xiao, S.-P. Sun, Z. Cui, Y. Wang, Unidirectional diffusion synthesis of covalent organic frameworks (COFs) on polymeric substrates for dye separation, J. Membr. Sci. 586 (2019) 274–280.
[15] S. Kandambeth, B.P. Biswal, H.D. Chaudhari, K.C. Rout, S. Kunjattu H., S. Mitra, S. Karak, A. Das, R. Mukherjee, U.K. Kharul, R. Banerjee, Selective molecular sieving in self-standing porous covalent organic framework membranes, Adv. Mater. 29 (2) (2017) 1603945, https://doi.org/10.1002/adma.v29.210.1002/adma.201603945.
[16] X. Shi, A. Xiao, C. Zhang, Y. Wang, Growing covalent organic frameworks on porous substrates for molecule-sieving membranes with pores tunable from ultra- to nanofiltration, J. Membr. Sci. 576 (2019) 116–122.
[17] H. Fan, J. Gu, H. Meng, A. Knebel, J. Caro, High-flux membranes based on the covalent organic framework COF-LZU1 for selective dye separation by nanofiltration, Angew. Chem. Int. Ed. 57 (15) (2018) 4083–4087.
[18] X. Shi, R. Wang, A. Xiao, T. Jia, S.-P. Sun, Y. Wang, Layer-by-layer synthesis of covalent organic frameworks on porous substrates for fast molecular separations, ACS Appl. Nano Mater. 1 (11) (2018) 6320–6326.
[19] J.L. Fenton, D.W. Burke, D. Qian, M. Olvera de la Cruz, W.R. Dichtel, Polycrystalline covalent organic framework films act as adsorbents, not membranes, J. Am. Chem. Soc. 143 (3) (2021) 1466–1473.
[20] I. Castano, A.M. Evans, H. Li, E. Vitaku, M.J. Strauss, J.-L. Brédas, N.C. Gianneschi, W.R. Dichtel, Chemical control over nucleation and anisotropic growth of two-dimensional covalent organic frameworks, ACS Cent. Sci. 5 (11) (2019) 1892–1899.
[21] A.M. Evans, L.R. Parent, N.C. Flanders, R.P. Bisbey, E. Vitaku, M.S. Kirschner, R. D. Schaller, L.X. Chen, N.C. Gianneschi, W.R. Dichtel, Seeded growth of single-crystal two-dimensional covalent organic frameworks, Science 361 (6397) (2018) 52–57.
[22] H. Yang, L. Yang, H. Wang, Z. Xu, Y. Zhao, Y. Luo, N. Nasir, Y. Song, H. Wu, F. Pan, Z. Jiang, Covalent organic framework membranes through a mixed-dimensional assembly for molecular separations, Nat. Commun. 10 (2019) 2101.
[23] H. Fan, A. Mundstock, A. Feldhoff, A. Knebel, J. Gu, H. Meng, J. Caro, Covalent organic framework-covalent organic framework bilayer membranes for highly selective gas separation, J. Am. Chem. Soc. 140 (32) (2018) 10094–10098.
[24] Y. Ying, M. Tong, S. Ning, S.K. Ravi, S.B. Peh, S.C. Tan, S.J. Pennycook, D. Zhao, Ultrathin two-dimensional membranes assembled by ionic covalent organic nanosheets with reduced apertures for gas separation, J. Am. Chem. Soc. 142 (9) (2020) 4472–4480.
[25] H. Yang, H. Wu, Y. Zhao, M. Wang, Y. Song, X. Cheng, H. Wang, X. Cao, F. Pan, Z. Jiang, Ultrathin heterostructured covalent organic framework membranes with interfacial molecular sieving capacity for fast water-selective permeation, J. Mater. Chem. A 8 (37) (2020) 19328–19336.
[26] A. Xiao, X. Shi, Z. Zhang, C. Yin, S. Xiong, Y. Wang, Secondary growth of bi-layered covalent organic framework nanofilms with offset channels for desalination, J. Membr. Sci. 624 (2021), 119122.
[27] C. Mao, S. Zhao, P. He, Z. Wang, J. Wang, Covalent organic framework membranes with limited channels filling through in-situ grown polyaniline for efficient dye nanofiltration, Chem. Eng. J. 414 (2021), 128929.
[28] G. He, S. Huang, L.F. Villalobos, M.T. Vahdat, M.D. Guiver, J. Zhao, W.-C. Lee, M. Mensi, K.V. Agrawal, Synergistic CO_2-sieving from polymer with intrinsic microporosity masking nanoporous single-layer graphene, Adv. Funct. Mater. 30 (2020) 2003979.
[29] Z. Zhang, C. Yin, G. Yang, A. Xiao, X. Shi, W. Xing, Y. Wang, Stitching nanosheets of covalent organic frameworks to build aligned nanopores in nanofiltration membranes for precise ion separations, J. Membr. Sci. 618 (2021), 118754.
[30] Z. Zhang, X. Shi, R. Wang, A. Xiao, Y. Wang, Ultra-permeable polyamide membranes harvested by covalent organic framework nanofiber scaffolds: a two-in-one strategy, Chem. Sci. 10 (2019) 9077–9083.
[31] J. Yuan, M. Wu, H. Wu, Y. Liu, X. You, R. Zhang, Y. Su, H. Yang, J. Shen, Z. Jiang, Covalent organic framework-modulated interfacial polymerization for ultrathin desalination membranes, J. Mater. Chem. A 7 (44) (2019) 25641–25649.
[32] N.A. Khan, J. Yuan, H. Wu, T. Huang, X. You, A.U. Rahman, C.S. Azad, M.A. Olson, Z. Jiang, Covalent organic framework nanosheets as reactive fillers to fabricate free-standing polyamide membranes for efficient desalination, ACS Appl. Mater. & Interfaces 12 (24) (2020) 27777–27785.
[33] N.A. Khan, H. Wu, Y. Jinqiu, W.u. Mengyuan, P. Yang, M. Long, A.U. Rahman, N. M. Ahmad, R. Zhang, Z. Jiang, Incorporating covalent organic framework nanosheets into polyamide membranes for efficient desalination, Sep. Purif. Technol. 274 (2021) 119046, https://doi.org/10.1016/j.seppur.2021.119046.
[34] D.B. Shinde, G. Sheng, X. Li, M. Ostwal, A.-H. Emwas, K.-W. Huang, Z. Lai, Crystalline 2D covalent organic framework membranes for high-flux organic solvent nanofiltration, J. Am. Chem. Soc. 140 (43) (2018) 14342–14349.
[35] D.B. Shinde, L.i. Cao, A.D.D. Wonanke, X. Li, S. Kumar, X. Liu, M.N. Hedhili, A.-H. Emwas, M. Addicoat, K.-W. Huang, Z. Lai, Pore engineering of ultrathin covalent organic framework membranes for organic solvent nanofiltration and molecular sieving, Chem. Sci. 11 (21) (2020) 5434–5440.
[36] C.Y. Tang, Y.-N. Kwon, J.O. Leckie, Probing the nano- and micro-scales of reverse osmosis membranes-a comprehensive characterization of physiochemical properties of uncoated and coated membranes by XPS, TEM, ATR-FTIR, and streaming potential measurements, J. Membr. Sci. 287 (2007) 146–156.